Design of a versatile clinical aberrometer

Matthew Sheehan, Alexander Goncharov, and Chris Dainty

Applied Optics, National University of Ireland – Galway

ABSTRACT

We have designed an ocular aberrometer based on the Hartmann-Shack (HS) type wavefront sensor for use in optometry clinics. The optical system has enhanced versatility compared with commercial aberrometers, yet it is compact and user-friendly. The system has the capability to sense both on-axis and off-axis aberrations in the eye within an unobstructed 20 degree field. This capability is essential to collect population data for off-axis aberrations. This data will be useful in designing future adaptive optics (AO) systems to improve image quality of eccentric retinal areas, in particular, for multi-conjugate AO systems. The ability of the examiner to control the accommodation demand is a unique feature of the design that commercial instruments are capable of only after modification. The pupil alignment channel is re-combined with the sensing channel in a parallel path and imaged on a single CCD. This makes the instrument more compact, less expensive, and it helps to synchronize the pupil center with the HS spot coordinate system. Another advantage of the optical design is telecentric re-imaging of the HS spots, increasing the robustness to small longitudinal alignment errors. The optical system has been optimized with a ray-tracing program and its prototype is being constructed. Design considerations together with a description of the optical components are presented. Difficulties and future work are outlined.

Keyword list: Hartmann-Shack, off-axis aberrations, aberrometer, design, multi-conjugate adaptive optics

1. INTRODUCTION

1.1 **Experiment Rationale**

In the last decade, wavefront sensing techniques have been applied to many investigations of monochromatic aberrations of the human eye[1]. The measurement of aberrations with a wavefront sensor is the first step in imaging with traditional adaptive optical (AO) systems. One of the most exciting fields that became possible with AO technology is high resolution imaging of the retina. A wealth of previously hidden detail can be extracted from the eye in vivo. Current AO imaging of the retina is limited to the fovea and parafoveal areas with fields of approximately 1 to 2 degrees[2]. Many efforts have gone into developing imaging modalities such as AO-Scanning Laser Ophthalmoscopy, AO-Optical Coherence Tomography, two-photon imaging and flood-illuminated imaging[3]. While these techniques improve resolution, it is anticipated that future techniques will improve contrast and allow diffraction limited imaging of retinal layers other than the photoreceptors, blood vessels and nerve fiber layer.

Apart from increased resolution and contrast in retinal imaging, one would also benefit from enlarging the field of view. Currently, wide field images are constructed by montage. The more advanced technique of multi-conjugate adaptive optics (MCAO) is a potential solution for wide field sensing and correction. To design efficient MCAO instruments for the eye, the range and type of aberrations typically occurring off-axis must be modeled. Previous studies of off-axis aberrations with the Hartmann-Shack (HS) sensor have been limited to small sample numbers[4] and thus more extensive experimental data is needed.

Wavefront sensing off-axis is more demanding than the regular on-axis case. In the off-axis case, the field of view of the fixation target and the dynamic range of the sensor become especially important parameters. We have constructed an ocular aberrometer of the HS type that is capable of measuring both on-axis and off-axis aberrations in the eye. The prototype system is being constructed with the aim of combining the features of a commercial instrument, such as: compact opto-mechanical design, large ammetropia range correction, and user-friendly interface, with the additional features of a research laboratory instrument, such as: high speed, off-axis capability, adjustable target settings, and source code flexibility. We present our optical design of a versatile HS wavefront sensor for the eye and discuss the some of the basic parameters that should be considered during the design process.

Optical Design and Engineering II, edited by Laurent Mazuray, Rolf Wartmann
Proc. of SPIE Vol. 5962, 59620M, (2005) · 0277-786X/05/$15 · doi: 10.1117/12.625093

2. DESIGN CONSIDERATIONS

2.1 **The Hartmann-Shack wavefront sensor**

The simplicity of the HS sensor makes it a popular choice for scientists investigating the eye. The basic principles of the HS sensor in eye applications can be summarized as follows: a fixation target is presented to the eye to control movement and accommodation. A narrow beam of light is focused onto the retina to form a spot. The small size of the beam and its central location at the pupil negates any wavefront distortion accumulated when passing into the eye. The scattered light passes back through the eye, exiting through the whole pupil, and accumulates aberrations due to imperfections in the optical elements of the eye. A lenslet array is conjugated to the pupil. Each lenslet samples the wavefront and creates an image of the retinal spot on a CCD camera. This array of images is compared to a reference measurement created by a plane wavefront. Aberrations within the instrument itself are accounted for by the reference image. The displacement of the spots with respect to their reference position allows calculation of the local slope of the wavefront over the sample. The local slopes (wavefront derivatives) are then integrated over the pupil to reconstruct the wavefront. Typically the wavefront is fitted to a set of Zernike polynomials. The coefficients of the polynomials are used to describe the contribution of individual aberrations (modes) to the overall wavefront error (departure from the ideal plane wavefront).

2.2 **Temporal sampling**

The temporal sampling, spatial sampling, dynamic range, sensitivity, and signal/noise requirements are all inter-related parameters and they must be balanced against each other for a given task.

The temporal sampling requirements in our design are slightly relaxed, since the wavefront sensor is not part of a closed AO loop. However, the system is fast enough to sense the most anticipated temporal events in the eye, such as blinking, ocular pulse, tear film degradation, fixational eye movements, accommodation, and contact lens movement. Tear film stability can have a time scale of only a few seconds, accommodation steady state micro-fluctuations occur with frequencies up to 3 Hz[5], a spontaneous blink occurs in about 260 ms, and involuntary micro-saccades have a time scale of about 20-800 ms[6]. Fixational tremors occur at frequencies between 40 and 100 Hz, but typically they have very small amplitudes (less than 1 arcmin). The value chosen for temporal sampling has implications for the CCD exposure time and power of the beam to ensure an adequate signal-to-noise ratio (SNR). Commercial HS sensors can capture frames at rates as fast as 10 Hz, but typically they operate at much lower speeds. Many research AO systems operate in closed loop at about 30 Hz. Researchers have shown[7,8] that much higher bandwidths are required to entirely sample the temporal envelope of ocular aberrations. Our first software development allows us to sense and display wavefront data at 10 Hz. Second stage software developments will provide more efficient algorithms for centroiding and wavefront reconstruction to improve temporal sampling without SNR compromise.

2.3 **Spatial sampling**

There are two principal restrictions in spatial sampling with the HS sensor. Firstly, the sample size must be small enough to satisfy the assumption that the wavefront can be accurately represented by a pure tilt over the sample. Secondly, sampling must be at such a high rate as to satisfy the Nyquist criterion during wavefront reconstruction to a given aberration order. We plan to fit reconstructed wavefronts to Zernike polynomials (from defocus up to 5^{th} order). We consider this to be a sufficient representation of the eye, because the magnitude of aberrations beyond 5^{th} order are likely to be comparable with instrumental accuracy. The highest sampling density in commercial HS wavefront sensors is 120 microns. Lower sampling density has the advantages of increased photon flux (therefore increased SNR) and reduced computational demand. On the other hand, higher sampling is particularly important for irregular eyes, such as post-operative eyes, keratoconic eyes, and in some dry eye conditions which have local distortions on scales less than the typical sample size (500 microns). The spatial sampling density of our instrument is 21 x 21 sub-apertures over an 8-mm pupil (380 microns). This is adequate to fit aberrations up to the fifth order even for pupils less than 4 mm in diameter.

2.4 **Dynamic range**

The dynamic range of the design allows measurement on a large proportion of the normal population and possibly sub-groups such as post-operative/irregular eyes. Off-axis sensing also requires a large dynamic range to account for the increased off-axis astigmatism. Statistics indicates that in most eyes the 2^{nd} order aberrations greatly exceed higher order aberrations. Therefore, it is practical to remove as much of the 2^{nd} order aberrations as possible before sensing the wavefront. Indeed HS principles rely upon the assumption that the wavefront sensed is almost plane and contains only small residual aberrations. Removing 2^{nd} order aberrations can be approached in many ways, each with its own merits

and limitations. A Badal optometer is used in our design to remove defocus. After pre-conditioning the wavefront with the Badal, the principle limitation of the sensor range is to restrict each spot within its designated sub-aperture. This restriction prevents confusion between neighboring spots. A scanning mask can avoid confusion of neighboring spots displaced outside their sub-apertures[9]. This increases the dynamic range, but reduces temporal sampling.

Prior knowledge is applied to make efficient use of the available sensor range. We rotate the lenslet array and CCD by 45 degrees around the line of sight of the eye. Since astigmatic correction is not incorporated into the Badal optometer (some wavefront sensor designs remove astigmatism with pre-conditioning cylindrical trial lenses or a pair of rotating cross cylinders), it will be the largest aberration required to be sensed in the majority of cases. It is a well-known fact that in human eyes astigmatism tends to be aligned with either the vertical or horizontal meridian rather than an oblique meridian. By rotating the lenslet array by 45 degrees, the instrument will sample less densely in the horizontal and vertical meridians by factor of 1.41, and the dynamic range is increased accordingly. Thus the meridian of maximum dynamic range of the sensor is matched to the typical meridians of maximum astigmatism in the eye. The dynamic range of our design transposes to –9.50DS / +13.00DS / –4.75DC for a 6-mm pupil, in traditional optometric terms, which compares favorably with commercial instruments.

2.5 **Sensitivity, eye safety and photon efficiency**

Sensitivity refers to the minimum local slope detectable over each sample. It is determined primarily by the pupil magnification, focal length of the lenslet array, SNR, the centroiding algorithm, and the number of pixels per spot width. Assuming SNR of 30:1 and neglecting speckle effects, our models predict instrument sensitivity to local slope higher than 10 arcsec. For the eye, HS sensors typically achieve a reasonable SNR even with a modest quality CCD. A good SNR is achievable while maintaining safe eye exposure levels[10], especially if the wavelength of the probing source is in the red-infrared region and matched to the quantum efficiency response curve of the CCD (typically exposures of less than 8 microwatts power are used for a red wavelength). In a second stage of software development, we plan to implement a maximum likelihood approach to determining the spot locations. This technique is potentially more accurate than conventional centroiding. Our design incorporates 29 optical surfaces between eye and CCD, which has a considerable impact on photon efficiency.

2.6 **Size and housing**

To use the instrument in a clinical setting, it must be compact and transportable. The mounts and assembly options were chosen to minimize the size and give the instrument stability. The optical design was optimized for compactness with compressed optical paths and a shared detector field. The final size of the instrument is 20cm x 36cm x 7cm. It is bracketed to an optical stage similar to that used by a keratometer or slit lamp. As such, the base has joystick control and 3 degrees of freedom. It incorporates a headrest and chinrest. In the future, we plan to introduce a nasal stabilizer device to improve subject stability without the discomfort associated with using a bite bar. The bracketing of the instrument to an optical table will make it transportable and give it a familiar aesthetic for both subjects and operators. The cage mounting system provides easy assembly and robust alignment.

2.7 **Wavelength range**

The wavelength choice for the probing source is determined by many factors. The red or infrared bandwidth is preferred because it provides a safety advantage and is more comfortable for the eye, therefore subjects are more likely to maintain accurate fixation. We use 670 nm, which compared to the fixation target (526 nm) should have minimal effects on accommodation, pupil size and fixation. Longer wavelengths have the benefit of greater retinal reflectance[11], but, it is also desirable to remain within the visible spectrum to avoid complications of invisibility during calibration and alignment. An additional benefit of separating the beacon and fixation wavelengths is the mild fogging effect that occurs as a natural consequence of chromatic aberration; the retinal spot remains in good focus even with a fogged fixation target. For longer wavelengths and for eyes with reduced ocular pigment, light penetrates deeper into the retina before reflection. This overestimation of myopia should in principle be taken into account when transposing wavefront data into refractive error data. However, the effect is outweighed by longitudinal chromatic aberration[1]. The 526-nm wavelength fixation target is close to the human spectral sensitivity peak, whereas the alignment arm operating at 890 nm avoids distracting the subject and prevents pollution of this source from altering the state of the eye such as accommodation, pupil size, and fixation.

3. OPTICAL SYSTEM COMPONENTS

3.1 **Fixation arm**

Provision of a fixation target is a fundamental requirement to control eye movement and accommodation. Important issues related to fixation include ammetropia range, fogging, spatial frequency content of target, and spectral frequency of the target illumination[12]. Figure 1 (a) shows the fixation arm of the instrument with rays traced for a 20-degree field. The 40-mm working distance is adequate for subject alignment and comfort. A plane parallel plate is used as a beamsplitter, its low reflectance of a few percent is adequate in providing a visible target under mesopic conditions. Off-axis sensing is performed by asking the subject to fixate on eccentric points on the target; the instrument is then realigned to the new pupil center position and measurements are taken. The target can translate along the optical axis and therefore it has focusing capability independent of the Badal optometer. This is advantageous because a fixation beam passing along the line of sight may need a different defocus settings compared to that required for the beacon wavefront traveling from an eccentric retinal location and exiting obliquely through the refractive elements of the eye. The target image is a reticule containing predominantly high spatial frequencies. It also incorporates an illusion-based scene to help control accommodation. The target is imprinted on a standard photographic negative (35 mm) and it is back illuminated by wide-angle LEDs operating at 526 nm. A slight curvature is introduced in the negative to compensate for the intrinsic field curvature of the fixation arm optics. Off-axis measurements at larger angles are possible by constructing fixation targets outside the instrument, for example on a screen a few meters behind the instrument.

For measurements involving on-axis aberrations and accommodation, one may utilize an alternative fixation target, which is presented to the eye via the Badal, so its defocus level is dependent upon the Badal setting. The alternative target is incorporated into the sensing arm in the plane of the diaphragm, see Fig. 2(a). This fixation target allows a 10-degree field of view. If fogging is required, the primary fixation target is more suitable than the alternative target.

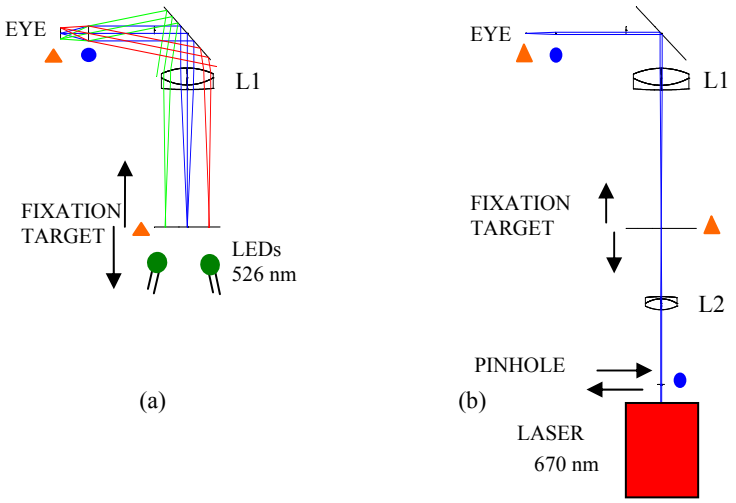

Fig. 1. Optical layout of the fixation arm (a) and probing arm (b). Retinal conjugates are shown by triangle icon. Pupil conjugates are shown by circle icon. The fixation target contains a small central aperture that allows the laser beam to pass unobstructed. The fixation target is translatable along the optical axis. The pinhole is translatable perpendicular to the optical axis.

3.2 **Probing arm**

Figure 1(b) illustrates the optical arrangement of the probing arm. Collimated light from the laser diode (670 nm) passes through the pinhole and it is focused to an intermediate plane coincident with the null position of the fixation target. The lens L1 re-collimates the laser light so that the eye can focus the beacon onto the retina. Lenses L1 and L2 provide optical conjugation of the pinhole to the pupil. To avoid unwanted reflection from the eye, the pinhole is decentered laterally from the optical axis. As a result, the 1.2-mm probing beam entering the eye is displaced by roughly 1 mm from the center of the pupil. Thus the reflections from the eye occur at skew angles and the diaphragm will block them. This issue of the back reflections is most critical for the design of the probing arm. Particularly problematic is the first Purkinje reflection (from the air/tear film interface) due to its high intensity. The laser output is linearly polarized and

aligned perpendicular to the reflection plane of the beamsplitter (a parallel plane plate). The low reflectance of the parallel plane plate (~4%) helps to attenuate the laser power to a safe emission level (the eye receives less than 8 microwatts). It also makes better use of the valuable photons returning from the retina (plate transmission ~96%) at the expense of surplus photons generated by the laser. The laser is not coupled to the movement of the fixation target, because even for ammetropic subjects the beacon size on the retina remains below the diffraction limit of the lenslets. The latter constraint is important to ensure that the beacon appears as a point source in each sub-aperture.

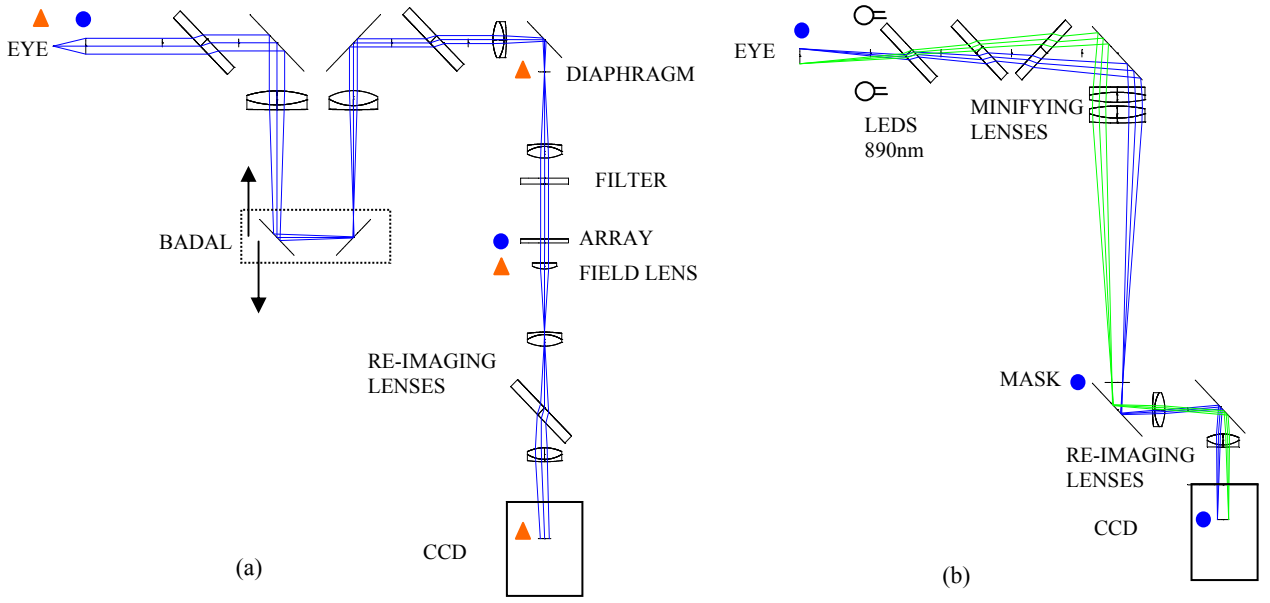

Fig. 2. Optical layout of the sensing arm (a) and alignment arm (b). Retinal conjugates are shown by a triangle icon. Pupil conjugates are shown by a circle icon. The diaphragm in (a) also acts as an alternative fixation target.

3.3 **Sensing arm**

The light scattered by the retina exits the eye, passes through the parallel plane plate, and then is reflected from a dichroic plate into the Badal optometer, see Figure 2(a). The focal length of lenses used in the Badal are chosen to satisfy the required beam magnification (at the lenslet array) and to provide a comfortable working distance to the subject. The Badal stage allows 105-mm translation, which is sufficient to vary the optical path length between the Badal lenses. For each subject, the Badal is set at a best defocus value to make efficient use of the instrument. In this case the wavefront reaching the lenslet array will be typically dominated by astigmatism. The polarization properties of the cornea can be used to partially reduce corneal back reflections, however, this technique is unnecessary in our design because a diaphragm is conjugated to the retina, thus providing superior control over back reflections. The diaphragm also acts as an alternative fixation target. A colored glass filter removes pollution from 526-nm light. The lenslet array has a 10-mm focal length, 190-micron pitch and a square geometry. The lenslet array and the CCD are rotated by 45 degrees to maximize the dynamic range of the sensor in the horizontal and vertical meridians as previously explained. The re-imaging magnification is selected to satisfy the required ratio between spot width and pixel size. The HS diffraction limited spot FWHM falls on approximately 3 x 3 binned pixels, which is appropriate for our centroiding algorithm. The design arrangement superimposing the alignment and the sensing images onto the CCD constrains the maximum and minimum pupil diameters measurable. As these limits are approached, the subject alignment needs to be more accurate. This is achievable with the optical stage mounting of the instrument.

In the absence of a field lens, the pupil conjugate would be re-imaged near the CCD, and the chief ray in each cone of light exiting the lenslets would arrive at an angle. Any misalignment of the CCD along the optical axis would cause transverse spot movements manifesting as defocus. To avoid this problem the field lens together with re-imaging lenses form a telecentric pass by conjugating the pupil to infinity. Thus all the chief rays become parallel to the optical axis when arriving at the CCD. An additional benefit is a reduced field curvature.

A combination of dichroic beamsplitters, mirrors and plane parallel plates are used to fold the optical paths and merge/split the various arms. The arrangement of elements at these junctions balance considerations of higher efficiency (achievable in reflection) with considerations of surface-induced wavefront distortion (minimized in transmission). The beamsplitters require high quality surfaces and consequentially have increased thickness. The beamsplitter thickness creates unwanted secondary effects including translation of the optical axis in transmission and ghosting in reflection. However, the reasonably symmetric arrangement of beamsplitters retains coincidence between the optical axis of the elements and the mechanical axis of the mounts for all except the two most distant elements; the eye and the final re-imaging lens. At these locations the optical axis is displaced 1.6 mm from the mechanical axis. Appropriate compensation in mechanical mounting is possible and we confirm this compensation in our prototype.

3.4 Alignment arm

An alignment arm is required for the examiner to correctly judge alignment and working distance. In this arm, the eye is illuminated by a ring of wide angle LEDs operating at 890nm, see Figure 2(b). The eye is illuminated by the infrared light and imaged by the instrument. Appropriate dichroic beamsplitters steer this arm to circumvent the Badal optometer and into a path parallel to the sensor arm before finally being superimposed onto the CCD. The alignment arm employs low reflection coefficients at various beamsplitters to attenuate intensity and avoid saturating the CCD. The large field of view (12 mm) in this arm provides the examiner with distinguishing landmarks for orientation and alignment of the subject/instrument. To limit pollution of the HS spots when superimposing the alignment image, an annulus mask is conjugated to the pupil to block a minimum central zone. This arrangement limits the pupil size measurable to diameters between 4 mm and 9 mm. A diaphragm (not shown in figures) positioned between the re-imaging lenses creates a telecentric pass. This restricts oblique rays, improving the final image and reducing the intensity. The alignment image will be used to determine the pupil center, which defines the origin of the wavefront coordinate system. It is expected that determining the pupil center in this manner will improve the accuracy of the wavefront reconstruction and modal fitting. Figure 3 shows the optical layout of the entire system.

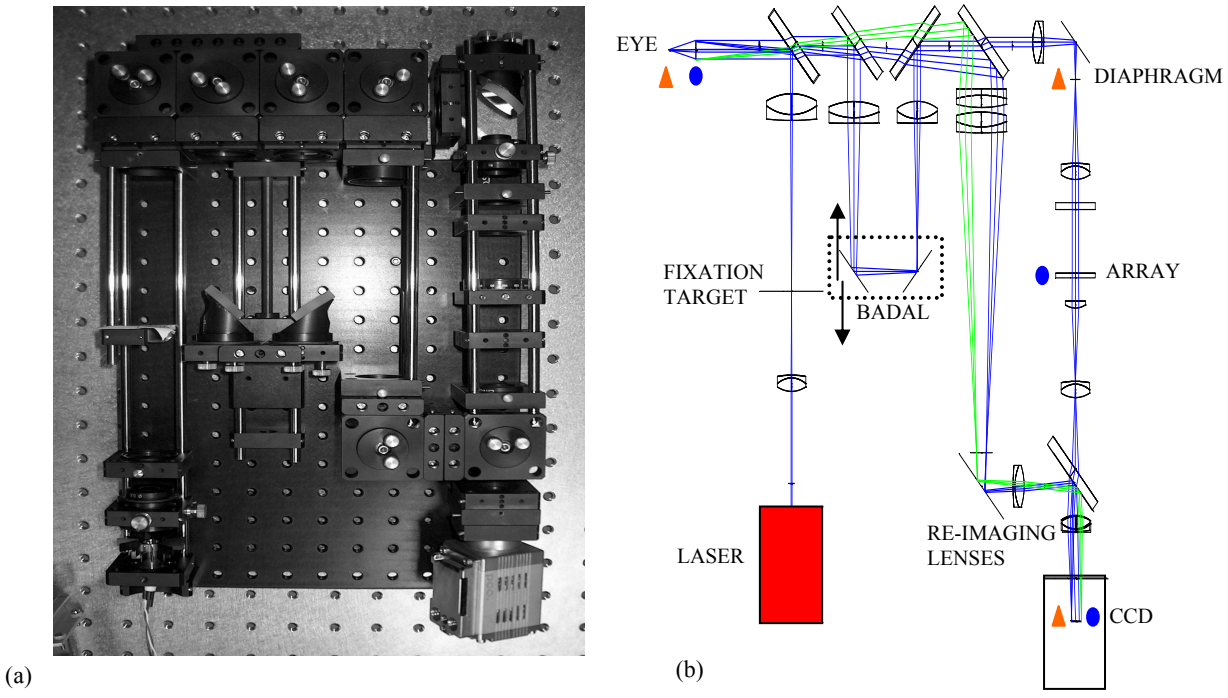

Fig. 3. Photograph (a) and schematic drawing (b) of the optical layout of a versatile Hatmann-Shack aberrometer.

4. DISCUSSION

4.1 **Comparisons with commercial and laboratory research aberrometers**

The design presented matches commercial aberrometers in terms of compact size, user-friendly operation, and large dynamic range. The instrument is small enough to be conveniently positioned in an eye clinic. It has a familiar aesthetic for both the operator and subject. The graphical user interface has been developed on a software platform that provides diverse display and database options. Desirable features of a research instrument have been achieved in the design such as off-axis capability and adjustable target settings. Our instrument speed is slower than comparable research wavefront sensors, however, for the initially planned studies the operational speed is not restrictive. Second stage development will give speed a higher priority.

4.2 **Versatile features of the design**

The ability to develop and alter the instrument in successive generations is an example of the advantage of having a versatile instrument in terms of physical mountings and software source code. Using only one CCD to image two optical paths makes the instrument more compact, less expensive, and easier to align coordinate systems between the two images (i.e. pupil center determination). Database management is also simplified as only one image file (containing HS spots and the eye position) is recorded per measurement. In the absence of trial lenses or rotating cross cylinders (to compensate for the astigmatic component of the wavefront), we use prior knowledge of ocular astigmatism to improve efficiency of the sensor range. By rotating both the lenslet array and CCD together as a single module by 45 degrees, the meridians of maximum dynamic range are matched to the meridians of maximum expected aberration. Telecentric imaging in both the sensing arm and the alignment arm is a nice optical feature, which improves robustness to misalignment.

5. CURRENT STATUS

5.1 **Prototype development**

The prototype is in the final stage of software development. A single platform runs all controls and operations such as: accepting operator commands, capture and record images, mathematical processing related to centroiding, wavefront reconstruction and Zernike mode fitting, graphical displays, and database management. The physical construction of the prototype is complete and shown in Figure 3(a).

5.2 **Difficulties and solutions**

The coherence of the laser and the diffuse scatter off the retina results in speckled HS spots. Speckle has a deleterious effect on centroiding and can be reduced by jittering the retinal spot or by increasing the exposure time and allowing retinal movement to decorrelate the speckle. However, the preferred method is to reduce the coherence length of the source by using a super luminescent diode (SLD) to create the retinal spot. Initially we experimented with an LED source to create the retinal spot in an effort to reduce speckles, while simultaneously reducing costs and simplifying the driver circuitry. Unfortunately, preserving the required parameters of a minimal retinal spot size, a narrow first pass beam width, a minimal exposure time, and maintaining the desired sample size proved too restrictive. The use of an LED to create the retinal spot is not abandoned, but as a temporary measure, we have installed the laser diode as presented in this paper. The laser will be upgraded to a SLD of a similar wavelength and bandwidth of approximately 50 nm in the near future.

Plate beamsplitters were used in the optical design because of their robustness and compact linear arrangement possible compared to pellicle and cube beamsplitters respectively. Mounting adjustments compensate for the translation of the optical axis, but the ghosting problem has not been overcome totally. For example, the probing beam entering the eye is actually composed of two beams, one from each reflection at each surface of the parallel plate (the ghost beam is not shown in figures). The beams straddle the optical axis and avoid Purkinje back reflections as intended, but the ghosting is an additional complication. We are considering future upgrades of replacing troublesome plate beamsplitters with pellicle beamsplitters.

In a well-designed HS wavefront sensor, a high SNR is usually achievable with a CCD of quite modest quality. We experimented with using a simple webcam in place of the scientific grade CCD. The webcam offered advantages of a

compact size and significantly reduced expense. Additionally, the webcam is powered and controlled by a single cable. Webcams are insensitive to infrared wavelengths although the units can be modified to resolve this problem. The main difficulty that prevented successful implementation was the cost of a software development kit. Third party software is available to grab individual display frames from a video stream, but we were not successful in accessing the original grey levels read from the chip. Because of these difficulties in driving the webcam, it is yet to be investigated weather the read noise of a webcam would be too high for our specific application.

6. FUTURE WORK AND CONCLUSIONS

6.1 **Conclusions**

Once the prototype is properly calibrated we will be able to present experimental accuracy and repeatability values. We plan to take advantage of the versatility in our design by locating the instrument within an optometry clinic. In the near future we expect to begin conducting studies of the monochromatic aberrations of various sub-populations. Future publications will present these results, the first of which will be a normal population study of the off-axis aberrations of the human eye.

The authors gratefully acknowledge the financial support of Science Foundation Ireland.

REFERENCES

1. D.A. Atchison, “Recent advances in measurement of monochromatic aberrations of human eyes,” Clin. Exp. Optom.; **88**, 5-27, 2005.
2. J. Liang, D. Williams, and D.T. Miller, “Supernormal vision and high-resolution retinal imaging through adaptive optics,” J. Opt. Soc. Am. **14**, 2884-2892, 1997.
3. J. Carroll, D.C. Gray, A. Roorda, D.R. Williams, “Recent advances in retinal imaging with adaptive optics,” Optics and Photonocs News, **16**, 36-42, 2005.
4. D.A. Atchison, and D.H. Scott, “Monochromatic aberrations of human eyes in the horizontal visual field,” J. Opt. Soc. Am. A **19**, 2180-2183, 2002.
5. W.N. Charman and G. Heron, “Fluctuations in accommodation: a review” Ophthalmic Physiol. Opt. **8**, 153-164, 1988.
6. S. Martinez-Conde, S.L. Macknik, D.H. Hubel, “The role of fixational eye movements in visual perception,” Nature, **5**, 229-240, 2004.
7. T. Nirmaier, G. Pudasaini, and J. Bille, “Very fast wave-front measurements at the human eye with a custom CMOS based Hartmann-Shack sensor,” Opt. Exp., **11**, 2704-2716, 2003.
8. L. Diaz-Santana, C. Torti, I. Munro, P. Glasson, and C. Dainty, “Benefit of higher closed-loop bandwidths in ocular adaptive optics,” Opt. Exp. **11**, 2597-2605, 2003.
9. Geunyoung Yoon’s web-page: http://www.cvs.rochester.edu/yoonlab/wavefront.htm.
10. European Committee for Electrotechnical Standardization, “Safety of laser products – user’s guide,” *IEC 60825-1:1993/A2:2001*, 69-93, National Standards Authority of Ireland, Dublin, 2001.
11. F.C.Delori, and K.P.Pflibsen, “Spectral reflectance of the human ocular fundus,” App. Opt., **28**, 1061-1077, 1989.
12. J. Schwiegerling, *Fieldguide to Visual and Ophthalmic Optics*, 19-26, SPIE press, Bellingham, 2004.